

## Supporting Information

### **Strain-free hybrid perovskite films based on molecular buffer interface for efficient solar cells**

Da Liu,<sup>‡a</sup> Mengjiong Chen,<sup>‡a</sup> Zhanpeng Wei,<sup>a</sup> Can Zou,<sup>a</sup> Xinyi Liu,<sup>a</sup> Jin Xie,<sup>a</sup> Qing Li,<sup>a</sup> Shuang Yang,<sup>\*a</sup> Yu Hou<sup>\*ab</sup> and Hua Gui Yang<sup>a</sup>

<sup>a</sup> Key Laboratory for Ultrafine Materials of Ministry of Education, Shanghai Engineering Research Center of Hierarchical Nanomaterials, School of Materials Science and Engineering, East China University of Science and Technology, Shanghai 200237, China, E-mail: syang@ecust.edu.cn; yhou@ecust.edu.cn

<sup>b</sup> Shenzhen Research Institute of East China University of Science and Technology, Shenzhen 518057, China

<sup>‡</sup>These authors contributed equally to this study.

## Experimental Section

**Materials:** Methylamine solution (33 wt% in absolute ethanol), lead iodide ( $\text{PbI}_2$ , 99%), isopropanol (99.5%) and dimethyl sulfoxide (DMSO, 99.9%) were purchased from Sigma-Aldrich. N,N-dimethylformamide (DMF, 99%), 2-methoxyethanol (2-me, 99%), tetrapentylammonium iodide (TPAI, 98%), and tetrahexylammonium iodide (THAI, 99%) were purchased from Alfa Aesar. Hydroiodic acid (HI, 57 wt% solution in  $\text{H}_2\text{O}$ ) and tetrabutylammonium iodide (TBAI, 99%) were purchased from J&K Scientific. Chlorobenzene (CB, 99.5%) was purchased from Aladdin. Ethanol (AR, 99.7%) was purchased from Shanghai Titan Technology Co. LTD. Nickel (II) acetate tetrahydrate, strontium chloride hexahydrate, and zinc powder were purchased from Sinopharm Chemical Reagent Co., Ltd. [6,6]-phenyl- $\text{C}_{61}$ -butyric acid methyl ester (PCBM, 99.5%) and bathocuproine (BCP, 99%) were purchased from Nichem chemicals. Fluorine-doped tin oxide (FTO) was purchased from Nippon Sheet Glass.

**Synthesis of methylammonium iodide ( $\text{CH}_3\text{NH}_3\text{I}$ ):**  $\text{CH}_3\text{NH}_3\text{I}$  was synthesized according to the reported method<sup>[1]</sup>. In a typical synthesis, 2 mL of HI and 4.8 mL of methylamine solution were dissolved in 20 mL ethanol. The mixture were stirred at 0 °C for 2 h in nitrogen atmosphere. White  $\text{CH}_3\text{NH}_3\text{I}$  precipitate was acquired by rotary evaporation of the mixed solution at 45 °C for 1 h, followed by drying at 60 °C in vacuum oven for 12 h.

**Device fabrication:** FTO substrate was patterned by etching with Zn powder and 2 M HCl diluted in deionized (DI) water. The etched FTO substrate was then cleaned by ultrasonication with acetone, ethanol, and DI water for 20 min, respectively. Then, the substrates were under UV ozone treatment for 15 min before spin coating  $\text{NiO}_x$  precursor solution. Pristine  $\text{NiO}_x$  films were deposited according to the reported method<sup>[2]</sup>. The  $\text{NiO}_x$  solution was prepared by dissolving nickel (II) acetate tetrahydrate in 2-me with concentration of 0.3 mol/L mixed with 5% molar ratios strontium chloride hexahydrate.  $\text{NiO}_x$  solution was spin-coated onto FTO at 3000 rpm for 30 s, followed by heated at 150 °C for 5min. After cooling to room temperature, the films were annealed at 500 °C for 1 h. For the buffer interface, TBAI, TPAI, and THAI were

dissolved in 2-me, respectively, with a concentration of 5 mg/mL. Then the solution was spin-coated at 3000 rpm for 30 s, followed by a heat treatment at 150 °C for 5 min. The  $\text{CH}_3\text{NH}_3\text{PbI}_3$  was deposited on the  $\text{NiO}_x$  film using a modified two-step method<sup>[3]</sup>. The 1.3 M  $\text{PbI}_2$  solution was prepared by dissolving 1.1986 g  $\text{PbI}_2$  in 2 mL of DMF and 185  $\mu\text{L}$  DMSO, stirring at 45 °C for 12 h. The solution was spin-coated on the  $\text{NiO}_x$  films at 3000 rpm for 30 s, and then spinning coating  $\text{CH}_3\text{NH}_3\text{I}$  (40 mg/mL in isopropanol) precursor on the top of the  $\text{PbI}_2$  film at 5000 rpm for 30 s, followed by annealing at 115 °C for 10 min. Afterwards, PCBM (20 mg/mL in CB) and BCP (0.5 mg/mL in ethanol) were spin-coated on the top of the  $\text{MAPbI}_3$  films at 2000 rpm for 45 s, and 4000 rpm for 45 s, respectively, and then annealed at 70 °C for 15 min. After cooling to room temperature, 100 nm of Ag was thermally evaporated as the back electrode.

**Characterization:** The morphology of modified  $\text{NiO}_x$  and perovskite films were characterized by field emission scanning electron microscopy (FESEM, HITACHI S4800). The crystallographic information of  $\text{PbI}_2$  and perovskite films were investigated by powder X-ray diffraction (PXRD, Bruker Advance D8 X-ray diffractometer, Cu  $K\alpha$  radiation, 40 kV). X-ray photoelectron spectroscopy (XPS, PHI5300, Mg anode, 250 W, 14 kV) was used to analyze the elemental composition of  $\text{NiO}_x$  and perovskite films. The transmittance spectra of modified  $\text{NiO}_x$  films and absorption spectra of  $\text{MAPbI}_3$  perovskite were measured by using a Cary 500 UV–vis–NIR Spectrophotometer. Solar cells were illuminated by a solar light simulator under AM 1.5 G irradiation ( $100 \text{ mW cm}^{-2}$ ) and the light intensity was calibrated to  $100 \text{ mW cm}^{-2}$  using a standard Newport calibrated KG5-filtered Si reference cell.  $J$ – $V$  curves of devices were measured with a Keithley 2400 digital source meter with a scan rate of  $0.15 \text{ V s}^{-1}$ . Devices were masked with a metal aperture to define the active area to be  $0.0625 \text{ cm}^2$ . The external quantum efficiency (EQE) was carried out on Zolix SCS 600 solar cell quantum efficiency measurement system. The steady state photocurrent output of the best-performing devices was measured by biasing the device at maximum power point for 600 s. Work function of the modified  $\text{NiO}_x$  films were measured by ultraviolet photoelectron spectrum (UPS) with He source of incident energy of 21.21

eV (He I line). The timeresolved photoluminescence (TRPL) spectra were acquired at room temperature using the Fluorolog-3-p spectrophotometer with an excitation wavelength of 460 nm. The electrochemical impedance spectra were measured out using an electrochemical workstation (Parstat 2273, Princeton) in the frequency range of 1.0 MHz and 1.0 Hz at 0.8 V under dark conditions. For contact angle measurement, water or DMF/DMSO droplets (about 5  $\mu$ L) were carefully dropped on the coated films by Dataphysics OCA20 contact-angle system, and measurements were processed at ambient atmosphere. For space-charge-limited-current (SCLC) measurement, the hole only structure device was fabricated with structure of FTO/NiO<sub>x</sub>/Perovskite/Spiro-OMeTAD/Ag. Current-voltage curves were recorded by Keithley 2400 digital source meter in the dark. The trap density was calculated as follows:

$$n_t = 2\varepsilon_0\varepsilon_r V_{TFL}/qL^2$$

where  $n_t$  is the trap density,  $\varepsilon_0$  is the vacuum permittivity,  $\varepsilon_r$  is the relative dielectric constant,  $V_{TFL}$  is the trap-filled limit voltage, and  $L$  is the thickness of film.

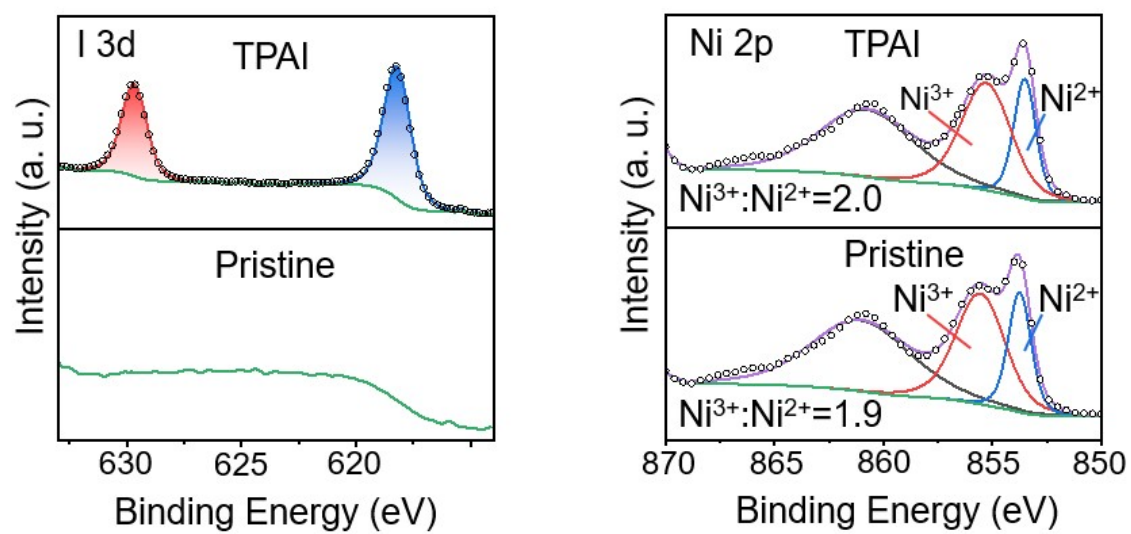


**Figure S1.** High resolution XPS spectra of I 3d (left) and Ni 2p (right) peaks of pristine and TPAI treated NiO<sub>x</sub> films.



**Figure S2.** Deionized water contact angle measurements of (left) NiO<sub>x</sub>, (middle) TPAI treated NiO<sub>x</sub> film. (right) TPAI treated NiO<sub>x</sub> film washed by the DMF/DMSO mixed solvent with volume ratio of 400:37.

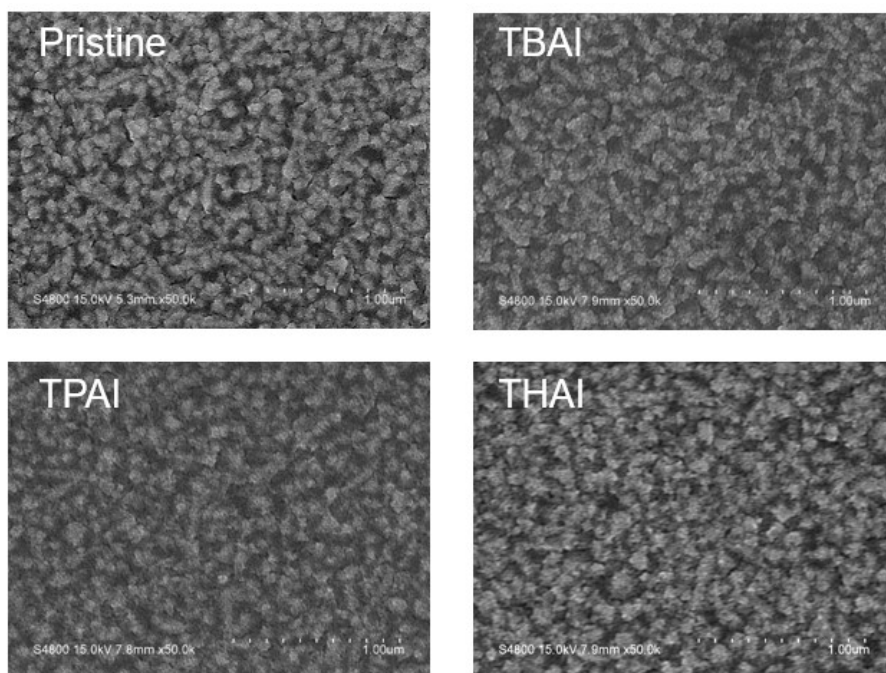


**Figure S3.** Top-view SEM images of NiO<sub>x</sub> films.

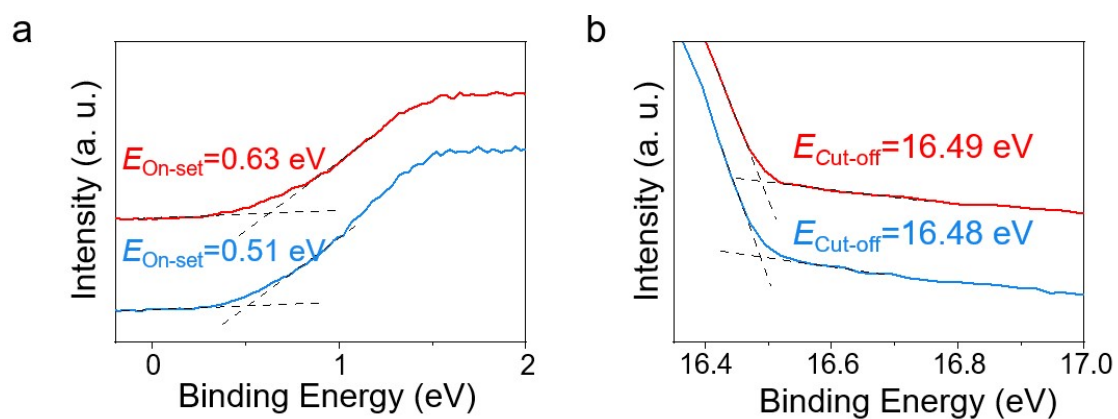


**Figure S4.** UPS (He I) spectra in the (a) onset ( $E_{\text{On-set}}$ ) and (b) cutoff ( $E_{\text{Cut-off}}$ ) energy boundary of the pristine (blue) and TPAI treated  $\text{NiO}_x$  films (red).

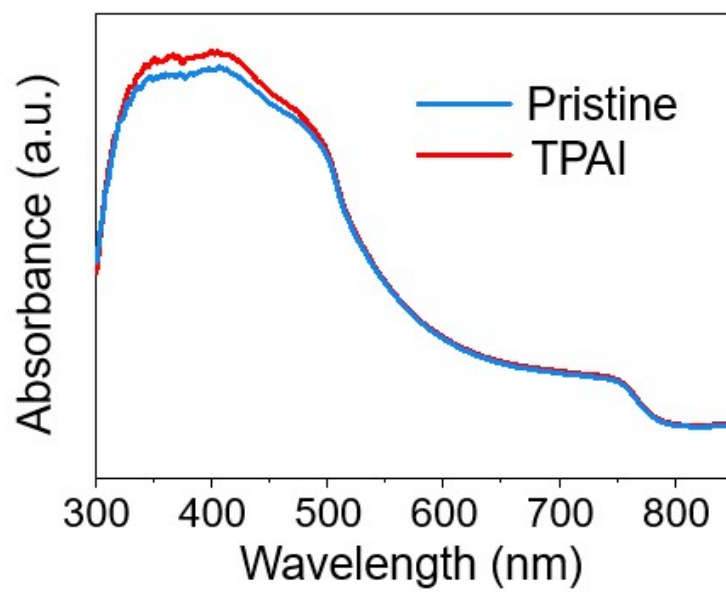


**Figure S5.** UV–vis absorbance spectra of perovskite films grown on pristine and TPAI treated  $\text{NiO}_x$  films.

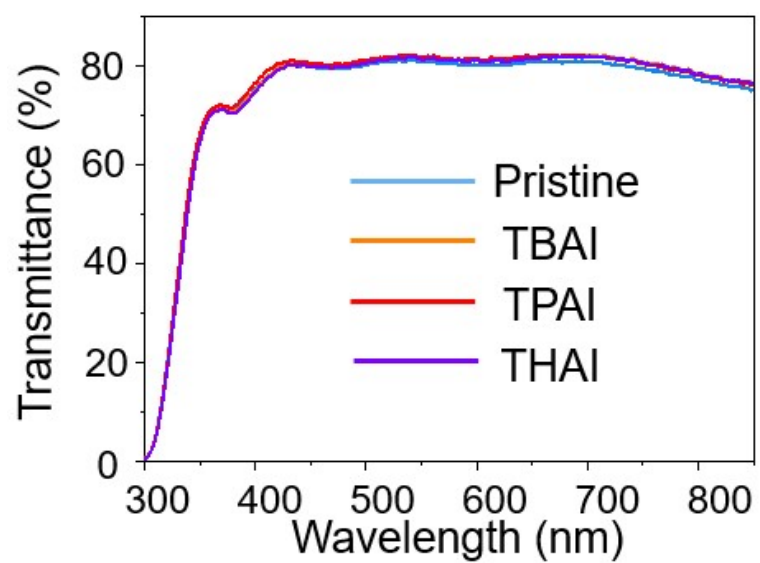


**Figure S6.** Optical transmission spectra of pristine and different alkyl ammonium iodide treated NiO<sub>x</sub> films. All samples deposited on FTO substrates.

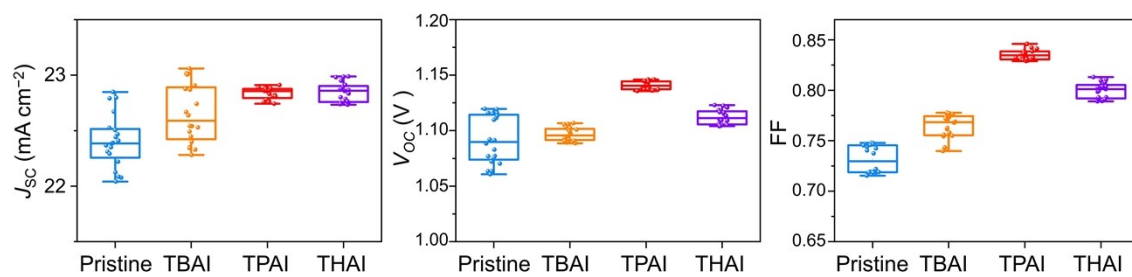


**Figure S7.**  $J_{sc}$ ,  $V_{oc}$  and FF distribution of PSCs with pristine and different alkyl ammonium iodide treated NiO<sub>x</sub> films.

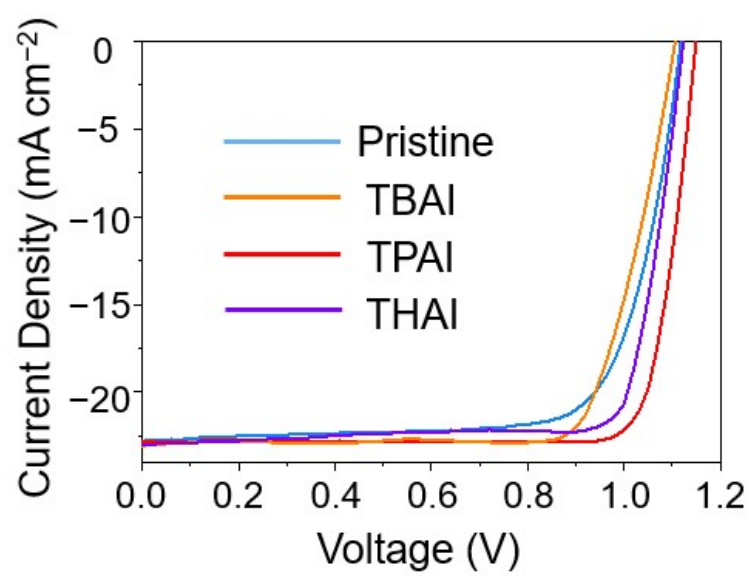


**Figure S8.**  $J$ - $V$  curves of PSCs with pristine and different alkyl ammonium iodide treated NiO<sub>x</sub> films.

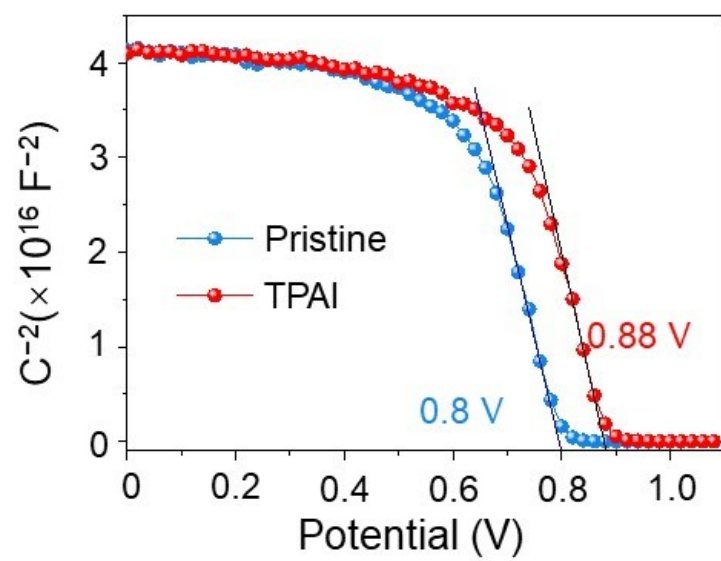


**Figure S9.** Mott-Schottky plots of devices with pristine and TPAI treated  $\text{NiO}_x$ .

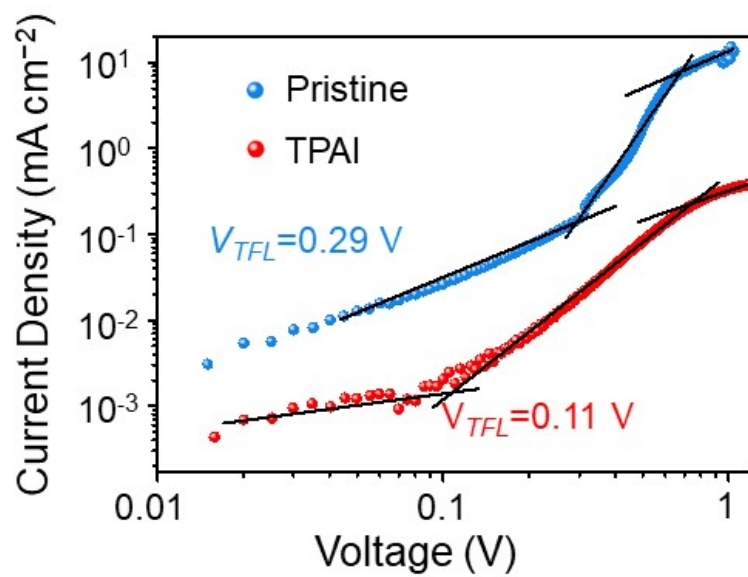


**Figure S10.** Dark  $J$ - $V$  curves of hole-only devices with pristine and TPAI treated  $\text{NiO}_x$  for SCLC.

The device structure is FTO/ $\text{NiO}_x$ /MAPbI<sub>3</sub>/Spiro-OMeTAD/Ag.

**Table S1.** Main device parameters for simulating perovskite solar cells. The values shown in brackets are specific for the pristine model.

| <b>Materials</b>  | <b>PCBM</b>                         | <b>MAPbI<sub>3</sub></b>            | <b>NiO<sub>x</sub></b>              | <b>PbI<sub>2</sub></b> |
|---|-------------------------------------|-------------------------------------|-------------------------------------|------------------------|
| <b>Thickness (nm)</b>   | 40 <sup>[4]</sup>                   | 480 (500)                           | 40                                  | 20                     |
| <b>Band gap (eV)</b>  | 1.8                                 | 1.5                                 | 3.7                                 | 2.48 <sup>[7]</sup>    |
| <b>Electron Affinity (eV)</b>   | 3.9 <sup>[4]</sup>                  | 3.9 <sup>[5]</sup>                  | 1.65                                | 3.35 <sup>[7]</sup>    |
| <b>Relative Permittivity</b>  | 3.75 <sup>[4]</sup>                 | 22 <sup>[5]</sup>                   | 11.75 <sup>[6]</sup>                | 20.8 <sup>[7]</sup>    |
| <b>CB effective density of states (cm<sup>-3</sup>)</b>                 | 2.5×10 <sup>19</sup> <sup>[4]</sup> | 2.2×10 <sup>18</sup> <sup>[5]</sup> | 2.5×10 <sup>20</sup> <sup>[6]</sup> | 1×10 <sup>20</sup>     |
| <b>VB effective density of states (cm<sup>-3</sup>)</b>                 | 2.5×10 <sup>19</sup> <sup>[4]</sup> | 2.2×10 <sup>18</sup> <sup>[5]</sup> | 2.5×10 <sup>20</sup> <sup>[6]</sup> | 1×10 <sup>20</sup>     |
| <b>Mobility (cm<sup>2</sup> V<sup>-1</sup> s<sup>-1</sup>)</b>          | 2×10 <sup>-3</sup> <sup>[4]</sup>   | 1 <sup>[5]</sup>                    | 1×10 <sup>-3</sup> <sup>[6]</sup>   | 1                      |
| <b>Shallow uniform donor density N<sub>D</sub> (cm<sup>-3</sup>)</b>    | 1×10 <sup>19</sup> <sup>[5]</sup>   | 1×10 <sup>12</sup> <sup>[5]</sup>   | -                                   | 1×10 <sup>12</sup>     |
| <b>Shallow uniform acceptor density N<sub>A</sub> (cm<sup>-3</sup>)</b> | -                                   | 1×10 <sup>12</sup> <sup>[5]</sup>   | 1×10 <sup>19</sup> <sup>[5]</sup>   | 1×10 <sup>12</sup>     |
| <b>Defect density (cm<sup>-3</sup>)</b>                                 | 1×10 <sup>15</sup>                  | 2×10 <sup>15</sup> <sup>[5]</sup>   | 1×10 <sup>15</sup>                  | 1×10 <sup>14</sup>     |

**Table S2.** Photovoltaic parameters of PSCs with various HTLs, simulated by the solar cell capacitor simulator.

| <b>HTLs</b>     | <b><math>J_{SC}^{a)}</math>/(mA cm<sup>-2</sup>)</b> | <b><math>V_{OC}^{b)}</math>/V</b> | <b>FF<sup>c)</sup></b> | <b>PCE/%</b> |
|-----------------|--|-----------------------------------|------------------------|--------------|
| <b>Pristine</b> | 22.93  | 1.13                              | 0.738                  | 19.13        |
| <b>TPAI</b>     | 23.02  | 1.20                              | 0.888                  | 24.53        |

<sup>a)</sup> Short-circuit current density; <sup>b)</sup> Open-circuit voltage; <sup>c)</sup> Fill factor.

**Table S3.** Photovoltaic parameters of PSCs with various HTLs, measured by reverse scan under simulated AM 1.5G solar irradiation.

| HTLs            |         | $J_{sc}/(\text{mA cm}^{-2})$ | $V_{oc}/\text{V}$ | FF    | PCE/% |
|-----------------|---------|------------------------------|-------------------|-------|-------|
| <b>Pristine</b> | Average | 22.40                        | 1.091             | 0.731 | 17.89 |
|                 | Highest | 22.79                        | 1.116             | 0.744 | 18.92 |
| <b>TBAI</b>     | Average | 22.65                        | 1.097             | 0.764 | 18.98 |
|                 | Highest | 23.06                        | 1.106             | 0.777 | 19.81 |
| <b>TPAI</b>     | Average | 22.83                        | 1.141             | 0.838 | 21.84 |
|                 | Highest | 22.83                        | 1.146             | 0.846 | 22.14 |
| <b>THAI</b>     | Average | 22.85                        | 1.112             | 0.800 | 20.32 |
|                 | Highest | 22.98                        | 1.123             | 0.813 | 20.98 |

**Table S4.** Photovoltaic parameters of the champion pristine and TPAI modified PSCs by forward and reverse scan.

| <b>HTLs</b>     | <b>Scan direction</b> | <b><math>J_{SC}/(\text{mA cm}^{-2})</math></b> | <b><math>V_{OC}/\text{V}</math></b> | <b>FF</b> | <b>PCE/%</b> |
|-----------------|-----------------------|--|-------------------------------------|-----------|--------------|
| <b>Pristine</b> | Reverse               | 22.79  | 1.116                               | 0.744     | 18.92        |
|                 | Forward               | 22.72  | 1.115                               | 0.740     | 18.74        |
| <b>TPAI</b>     | Reverse               | 22.83  | 1.146                               | 0.846     | 22.14        |
|                 | Forward               | 22.96  | 1.142                               | 0.833     | 21.85        |

## References

- [1] T. Y. Wen, S. Yang, P. F. Liu, L. J. Tang, H. W. Qiao, X. Chen, X. H. Yang, Y. Hou, H. G. Yang, *Adv. Energy Mater.*, 2018, **8**, 1703143.
- [2] B. Ge, H. W. Qiao, Z. Q. Lin, Z. R. Zhou, A. P. Chen, S. Yang, Y. Hou, H. G. Yang, *Sol. RRL*, 2019, **3**, 1900192.
- [3] M. Chen, H. W. Qiao, Z. Zhou, B. Ge, J. He, S. Yang, Y. Hou, H. G. Yang, *J. Mater. Chem. A*, 2021, **9**, 9266–9271.
- [4] D. Glowienka, Y. Galagan, *Adv. Mater.*, 2022, **34**, 2105920.
- [5] J. Diekmann, P. Caprioglio, M. H. Futscher, V. M. Le Corre, S. Reichert, F. Jaiser, M. Arvind, L. P. Toro, E. Gutierrez-Partida, F. Peña-Camargo, C. Deibel, B. Ehrler, T. Unold, T. Kirchartz, D. Neher, M. Stollerfoht, *Sol. RRL*, 2021, **5**, 2100219.
- [6] E. Raza, Z. Ahmad, F. Aziz, M. Asif, A. Ahmed, K. Riaz, J. Bhadra, N. J. Al-Thani, *Sol. Energy*, 2021, **225**, 842–850.
- [7] C. Luo, Y. Zhao, X. Wang, F. Gao, Q. Zhao, *Adv. Mater.*, 2021, **33**, 2103231.